Trace metal fractional solubility in size-segregated aerosols from the tropical eastern Atlantic Ocean

Alex R. Baker [1], Mingpei Li [1,†], Rosie Chance [1,‡]

[1]Centre for Ocean and Atmospheric Science, School of Environmental Sciences, University of East Anglia, Norwich, NR4 7TJ UK

† current address: Interdisciplinary Computing and Complex Biosystems, Newcastle University, Newcastle upon Tyne, NE1 7RU UK

‡ current address: Wolfson Atmospheric Chemistry Laboratories, Department of Chemistry, University of York, Heslington, York, YO10 5DQ UK

Corresponding author: Alex Baker (alex.baker@uea.ac.uk)

Key Points:

The solubility in fine fractions of Saharan dust aerosols is enhanced for Fe, Al and Ti, but not for Mn, Co and Th.
Fe, Al and Ti solubility increases strongly during atmospheric transport of dust, while Mn, Co and Th solubility does not.
The stability of Th solubility during transport may make it a more suitable tracer for dust inputs to the ocean than Al or Ti.

Abstract

Soluble and total trace metals were measured in size fractionated aerosol samples collected over the tropical eastern Atlantic Ocean. In samples that were dominated by Saharan dust, the size distributions of total iron, aluminium, titanium, manganese, cobalt and thorium were very similar to one another and to the size distributions of soluble manganese, cobalt and thorium. Finer particle sizes (< ~3 μm) showed enhanced soluble concentrations of iron, aluminium and titanium, possibly as a result of acid processing during atmospheric transport. The difference in fine particle solubility between these two groups of elements might be related to the hyperbolic increase in the fractional solubility of iron, and a number of other elements, during the atmospheric transport of Saharan dust, which is not observed for manganese and its associated elements. In comparison to elements whose solubility varies during atmospheric transport, the stability of thorium fractional solubility should reduce uncertainties in the use of dissolved concentrations of this element in seawater as a proxy for dust deposition.

1 Introduction

Atmospheric deposition of mineral dust is an important source of trace elements to the remote surface ocean. Many of these trace elements (e.g. iron (Fe), phosphorus (P), cobalt (Co), manganese (Mn), copper (Cu)) are essential components of marine microbial metabolic systems (Mahowald et al., 2018) and thus the deposition of dust plays a significant role in phytoplankton growth and the cycling of carbon in the ocean and the Earth System as a whole (Jickells et al., 2005).

The solubility (the fraction of their total atmospheric input that dissolves) of these trace elements is key to their impact on microorganisms, because in most cases it is soluble forms that are available for incorporation into cells (e.g. Morel et al., 2008). There is a large body of evidence that indicates that the solubility of Fe increases hyperbolically as total Fe atmospheric concentration decreases (i.e. with transport away from dust source regions) (Baker & Jickells, 2006; Chen & Siefert, 2004; Jickells et al., 2016; Shelley et al., 2018; Sholkovitz et al., 2012). Similar hyperbolic relationships between solubility and atmospheric concentration have been reported for many other dust-associated elements, e.g. aluminium (Al), silicon (Si), P, titanium (Ti) and lead (Pb) (Baker & Jickells, 2006; Prospero et al., 1987; Shelley et al., 2018).

Attempts to understand this solubility behaviour have focussed largely on Fe (Aguilar-Islas et al., 2010; Baker & Jickells, 2006; Sedwick et al., 2007; Sholkovitz et al., 2012; Spokes et al., 1994), because of its major role as a limiting nutrient over large regions of the global ocean (Jickells et al., 2005). Consideration of additional trace elements can help to evaluate the relative importance of potential controls on solubility (Baker et al., 2014), as well as shed light on the biogeochemical cycles of these other species. When trace elements delivered with dust (such as Al, Ti and thorium (Th)) do not have a significant metabolic function or other confounding factor, their surface water dissolved concentrations can be used to estimate dust flux and hence the atmospheric supply of associated bioactive elements (Anderson et al., 2016). The fractional solubility of these tracer elements in dust is a key uncertainty in these calculations (Anderson et al., 2016; Hsieh et al., 2011; Measures et al., 2010).

Not all elements exhibit significant increases in solubility with decreasing atmospheric dust concentration. The solubility of Mn in Saharan dust aerosols has been reported to vary little with dust (total Mn) concentration (Jickells et al., 2016; Shelley et al., 2018) and similar behaviour has been observed for Co (Shelley et al., 2018).

In this work, the solubilities of several mineral dust-associated trace elements (Fe, Al, Ti, Mn, Co, Th) have been examined in size fractionated aerosol samples collected over the tropical Atlantic Ocean. The overall (summed over all size fractions) solubility observed in these samples is compared to that of other non-size fractionated Saharan dust aerosols. Variations in solubility with particle size are discussed in terms of the influences on dust solubility of weathering in source regions and atmospheric processing. The impact of variations in solubility on the suitability of trace elements as proxies for Saharan dust deposition is also considered.

2 Materials and Methods

Size segregated aerosol samples were collected during two cruises in 2011 in the eastern tropical Atlantic Ocean aboard RRS *Discovery* (Figure 1). Cruise D361 (GEOTRACES section cruise GA06) took place in February – March (Jickells et al., 2016), while D371 (AMT21) crossed the north Atlantic in October as part of the Atlantic Meridional Transect (AMT) programme (Baker & Jickells, 2017). Most aerosol sampling during these cruises was done using Sierra-type cascade impactors to separate the collected material into two size classes, with a boundary at an aerodynamic diameter of ~ 1 μm. However, the 4 samples discussed here were collected using multiple impactor stages to give more detailed information on the size distribution of aerosol components (Table 1). Soluble trace metals were extracted from aerosol samples using ammonium acetate solution at pH 4.7, while leaching with ultrapure water was used for major ion (including sodium, nitrate, sulphate and oxalate) extraction. The application of these methods to the samples collected during AMT21 and D361 have been described previously (Baker & Jickells, 2017; Bridgestock et al., 2017; Jickells et al., 2016).

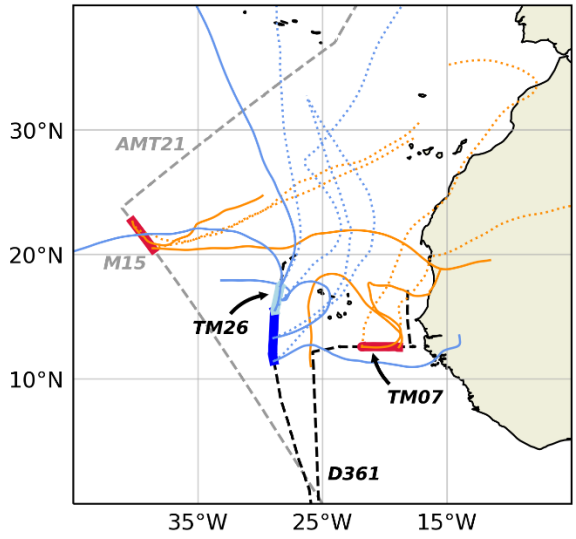

Figure 1 Tracks of the D361 (black) and AMT21 (grey) cruises through the eastern north Atlantic. Aerosol collection periods are indicated by thick solid lines (red for samples with high concentrations of mineral dust, blues for other samples). 5 day air mass back trajectories are shown as dotted lines for arrivals 10 m above the ship's position and solid lines for 1000 m arrivals. Back trajectories extend beyond the boundaries of the map in some cases.

Table 1 Cascade impactor stages used during the D361 and AMT21 cruises, and their associated particle size cut-offs (aerodynamic diameter) at the collector flow rate used, 1 m^3 min^{-1}. Backup filters (stage w in Figures 3 – 5) collected particles smaller than the cut-off for the last impactor stage.

a – not used for TM sampling during AMT21.

Impactor stage	**Cut-off diameter (µm)**
1	7.8
2	3.3
3	1.65
4	1.09
5	0.61
6 [a]	0.36

The total metal composition of the multi-stage samples was determined after a strong acid digestion procedure using 15.4 M HNO_3 (TraceSELECT™, for trace analysis, ≥69.0%, Honeywell Fluka™) and 27-30 M HF (47-51%, Trace Metal™, for Trace Metal Analysis, Fisher Chemical). Portions of each collection substrate were placed in acid-washed Teflon beakers and evaporated gently to dryness after sequential additions of 5 mL HNO_3, 1 mL HF and 1 mL HNO_3 on a ceramic hotplate (Baker et al., 2006). The hotplate was housed inside a plastic box, which was placed in a fume cupboard. Fumes from the digestion were drawn through a saturated solution of $CaCO_3$ in order to remove any excess HF from the vented air flow. Once digestion was complete, the residues were redissolved in 0.15 M HNO_3, quantitatively transferred to acid-washed 50 mL polypropylene centrifuge tubes and left to stand for 24 hours before filtration through 0.2 µm cartridge filters (cellulose acetate, Sartorius). Blank digestions and digestions of Arizona Test Dust (20 – 24 mg) were performed with each batch of aerosol digests. Results obtained for Arizona Test Dust are presented in Table 2.

Table 2 Mean and standard deviation elemental composition of Arizona Test Dust determined in this study (n = 5).

Element	Concentration (ppm)
Fe	28600±1100
Al	60300±3500
Ti	2510±100
Mn	658±34
Co	15.0±0.5
Th	16.0±0.7

Trace element concentrations in the filtered digests were determined by ICP-MS (iCAP TQ, Thermo Scientific) using rhodium as an internal standard. Calibration solutions were prepared from SPEX CertiPrep stock solutions. Certified reference materials (TM27.3 and TMDA64.2, Environment Canada) were analysed together with each batch of samples. Recoveries for certified elements in these standards were within 5 % (Fe, Mn, Co) and 10 % (Al, Ti). Reference values for Th in these CRMs are not available. Blank values and detection limits impactor stages and backup filters are given in Table S1.

Fractional solubility for each element was calculated as the ratio of its soluble to total concentration, expressed as a percentage. Separation of aerosol samples into multiple size fractions results in a lower sample loading per stage, and hence an increased likelihood of components in individual size fractions being below the limit of detection, particularly when total aerosol trace metal concentrations are low (Sakata et al., 2018). If both soluble and total concentrations were below the detection limit, solubility was not calculated. In cases where either one of the measured values was below detection limit, the detection limit was substituted for the missing value in the calculation. The calculated solubility was therefore an upper limit if the soluble concentration was below detection, and a lower limit if the total concentration was below detection. Where below detection limit values were present in the calculation of properties summed over sample size fractions (e.g. in Table 3), missing values in the summation were replaced with 75% of the relevant limit of detection. If more than one below detection limit value was present in such a calculation, their contribution to the total was taken to be the square root of the sum of their squares (i.e. they were treated as uncertainties). In order to account for these corrections in the uncertainty in the summed value, for each below detection limit value in a calculation the associated uncertainty was taken to be 100% of the relevant detection limit.

Air mass back trajectories were calculated for the 5 days prior to sample collection at heights of 10, 500 and 1000 m above the ship's position using the READY Hysplit archived trajectory model (Draxler & Rolph, 2003).

3 Results and Discussion

3.1 Properties of size-fractionated samples

Two of the samples reported here (AMT21 M15 and D361 TM07) exhibited the orange/brown colouration associated with mineral dust aerosols on several of their upper impactor stages. Air mass back trajectories for these samples (Figure 1) indicated passage of air over regions in Mauritania that have been identified as active dust sources (Stuut et al., 2005). The other samples collected during D361 (TM25 & TM26) did not show dust colouration, had air mass arrivals predominantly from the north and their total (summed over all size fractions) concentrations of dust-associated trace elements were at least an order of magnitude lower than samples M15 and TM07 (Table 3). Based on their respective concentrations of soluble Na^+ and total Al, the mass ratios of seaspray to mineral dust in the samples were 0.13 (M15), 0.34 (TM07), 13.2 (TM25) and 6.0 (TM26). Mineral dust was therefore a relatively minor constituent of samples TM25 &

TM26. Isotopic analysis of samples collected concurrently with TM07 and TM25 + TM26 combined also suggests that mineral dust contributed a greater proportion of Pb to sample TM07 than during the latter period (Bridgestock et al., 2016).

The concentrations of dust-associated elements in samples M15 and TM07 were within a factor of 2 of each other (Table 3). The lower concentrations observed in sample M15 may have been partly due to deposition along its probable longer atmospheric transport pathway (M15 was located ~2200 km west of the coast of Western Sahara, while TM07 was collected ~350 km west of Senegal, although actual transport pathways from source regions will be longer than this). Differences in the relative proportions of dust-associated elements in the different size fractions of these two samples may also be due to changes during transport. For instance, the proportions of total Fe found in the > 7.8 μm (stage 1) and < 0.61 μm (stages w & 6) fractions in TM07 were 13.7% and 9.7 % respectively, while the corresponding values for M15 were 5.5% and 26.2%. These differences would be consistent with preferential deposition of larger dust particles during transport (Ryder et al., 2013).

Table 3 Sum of the total concentrations of trace elements over all size fractions for the aerosol samples considered here, and the overall solubility of those trace elements in each sample.

Sample	Element	Total Conc. (pmol m^{-3})	Overall Sol. (%)	Element	Total Conc. (pmol m^{-3})	Overall Sol. (%)
M15	Fe	20000±130	1.09±0.06	Mn	323±3	43.3±1.6
	Al	74200±570	2.05±0.07	Co	8.6±0.5	19.0±1.1
	Ti	1620±14	0.167±0.016	Th	1.85±0.11	6.6±0.4
TM07	Fe	32800±200	1.08±0.05	Mn	614±5	46.4±0.5
	Al	126000±1000	2.04±0.02	Co	15.3±0.8	27.2±1.5
	Ti	2640±20	0.094±0.005	Th	3.09±0.15	7.9±0.7
TM25	Fe	724±6	2.32±0.26	Mn	22.6±0.3	71.9±1.0
	Al	3160±50	7.75±0.16	Co	0.43±0.05	29.2±4.0
	Ti	92.1±1.9	<0.139	Th	0.089±0.016	4.9±1.0
TM26	Fe	1140±6	<0.88	Mn	21.2±0.3	35.2±0.8
	Al	4600±50	4.23±0.13	Co	0.73±0.06	15.7±1.6
	Ti	98.5±2.0	<0.203	Th	0.14±0.02	3.6±0.8

3.2 Solubility – concentration relationships of non-fractionated dust aerosols

Figure 2 shows the overall solubility (i.e. the average solubility across all size fractions) of Fe, Al, Ti, Mn, Co and Th in the samples studied here, together with previously reported data for

177 Saharan dust aerosols collected over the Atlantic Ocean for which soluble element
178 concentrations were determined by the same extraction protocol used here (Jickells et al., 2016).
179 Dust concentration (calculated from total Al concentration) is plotted on the x-axes of Figure 2,
180 rather than total element concentration, for convenience. This truncates the range of values on
181 the x-axes, but does not otherwise alter the plots. The data are plotted on both log and linear
182 scales to emphasise the differences in behaviour between Fe / Al and Mn (n = 124 for these
183 elements). There are fewer observations available for Ti, Co and Th (n = 14), but the latter two
184 elements appear to behave similarly to Mn, with very little variation in solubility with dust (total
185 element) concentration. Shelley et al. (2018) reported that the solubility of Co varied more
186 strongly with total Co concentration in Saharan dust aerosols when ultrapure water was used to
187 leach the soluble element than it did when acetic acid was used as the leaching solution. The data
188 for Ti are rather scattered, and it is not possible to state, based on Figure 2, whether this
189 element's variation in solubility with dust concentration is hyperbolic or less variable. However,
190 Ti has been shown to have a hyperbolic solubility – concentration relationship in other Saharan
191 dust aerosols (Shelley et al., 2018).
192

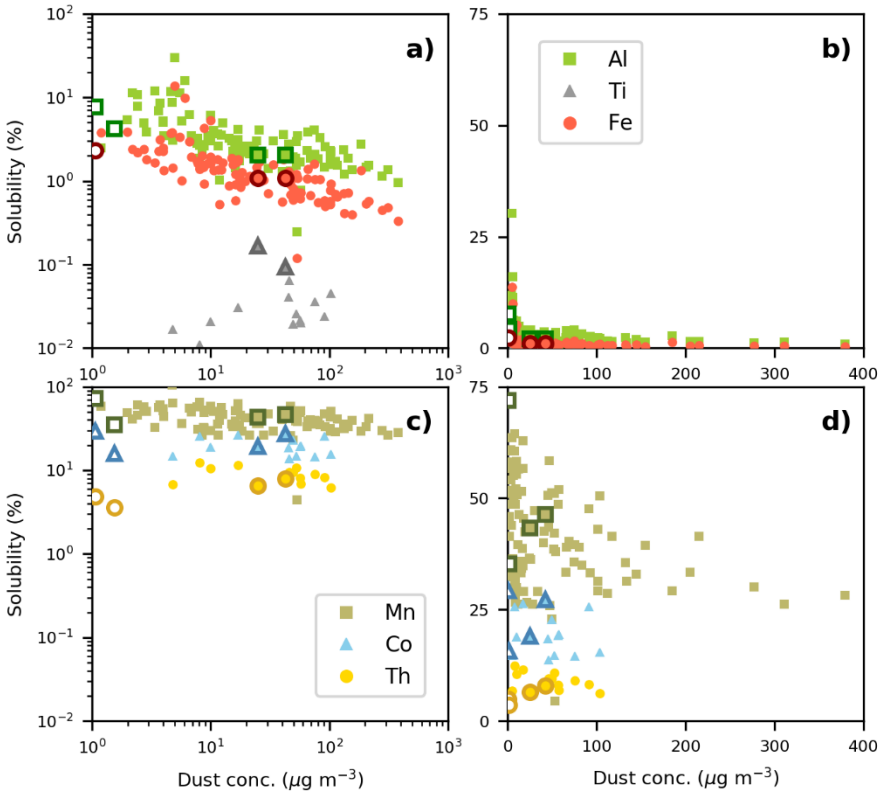

193 **Figure 2** The variation in fractional solubility with atmospheric dust concentration for Fe, Al and
194 Ti (a & b) and Mn, Co and Th (c & d) in Saharan dust aerosols sampled over the Atlantic Ocean
195 (Jickells et al., 2016). Values for the size-segregated samples examined in this work (Table 3) are
196 indicated with larger symbols. All other data for Ti, Co and Th are from D361. (Data are plotted
197 on log scales in a & c and linear scales in b & d).

198

199 *3.3 Solubility of size-fractionated samples*

200 Within each of the dusty samples, the distributions of the total concentrations of Fe, Al, Ti, Mn,
201 Co and Th (as well as P and chromium, not shown) across the size fractions were very similar
202 (Figure 3a & b), providing further evidence that dust was the dominant source of these elements
203 in those samples. Although absolute concentrations were much lower (Table 3), total element
204 distributions in sample TM25 (Figure 3c) were also similar to those in TM07, which may
205 indicate that some dust was present (as hinted at by high-level air mass arrivals from Mauritania
206 early in the collection period, Figure 1). Total element distributions in sample TM26 indicate
207 higher proportions in particles smaller than ~3 μm (Figure 3d). Broadly similar size distributions

of total Fe have been reported in Saharan dust-dominated and northerly marine-influenced aerosol samples in this region of the North Atlantic (Buck et al., 2010).

The size distributions of soluble Mn, Co and Th in TM07 and M15 are also essentially the same as their total element distributions, but this is not the case for the other soluble elements in these samples (Figure 3e & f). In particular, the relative soluble concentrations of Fe and Al were much higher in particles smaller than ~1.65 µm (stages w – 4), than were their relative total concentrations. Due to their much lower overall concentrations, soluble concentrations in samples TM25 and TM26 were not always detectable. (Below detection limit concentrations are not plotted in Figure 3g & h for clarity, but all relevant values are included in Table S1). Partly because the size distributions of the elements' total concentrations were less uniform than for the dusty samples, and partly because there was less data available for the soluble elements, it is difficult to discern whether Fe and Al soluble concentrations are enhanced in the finer fractions of the non-dusty samples.

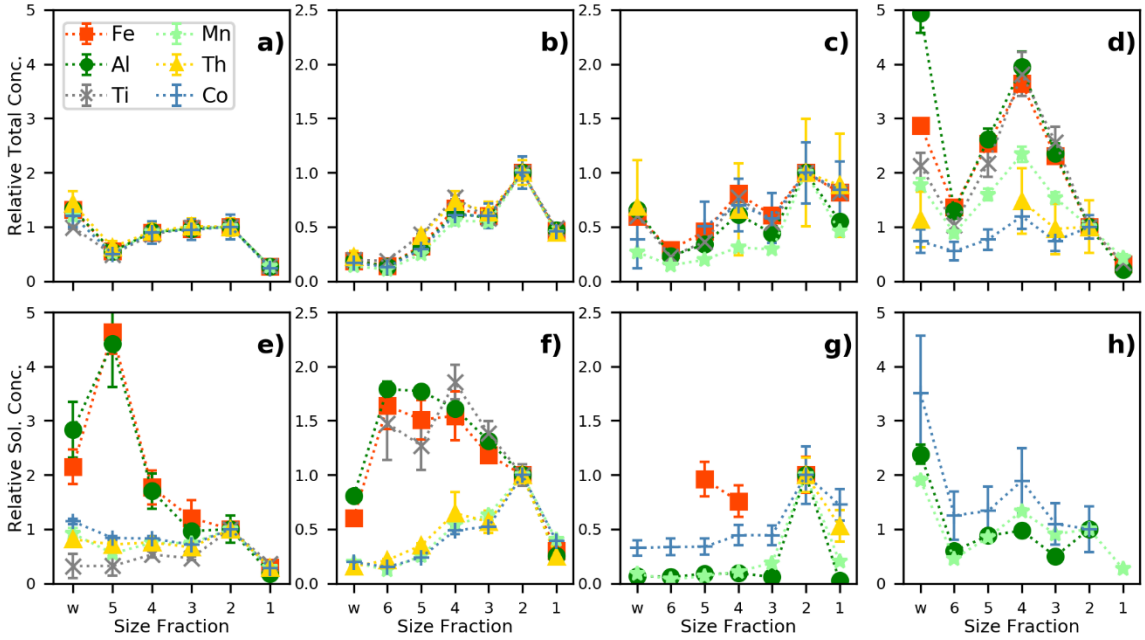

Figure 3 Concentrations of total (a - d) and soluble (e - h) elements in each aerosol size fraction normalised to their respective concentrations in impactor stage 2 for samples M15 (a & e), TM07 (b & f), TM25 (c & g) and TM26 (d & h). (Numbers on x-axis refer to the cascade impactor stages (Table 1), and w to the backup filter).

As a result of the differences in the soluble concentrations, there are some striking differences in the variation of fractional solubility across the aerosol size distribution for the two groups of elements (Figure 4). The profiles of Mn, Co and Th solubility are relatively flat across the size range, while those of Fe, Al and Ti show distinct maxima in the smaller size fractions, especially for the dusty samples. Buck et al. (2010) have also reported that the solubility of Fe was higher in particles in the ~0.3 – 1 µm size range than in larger (> ~3 µm) particles in dust-dominated aerosols over the tropical Atlantic, and Ooki et al. (2009) reported higher Fe solubility (up to 12%) in fine (< 3.3 µm) fractions of Asian mineral dust aerosol collected at Hokkaido, Japan.

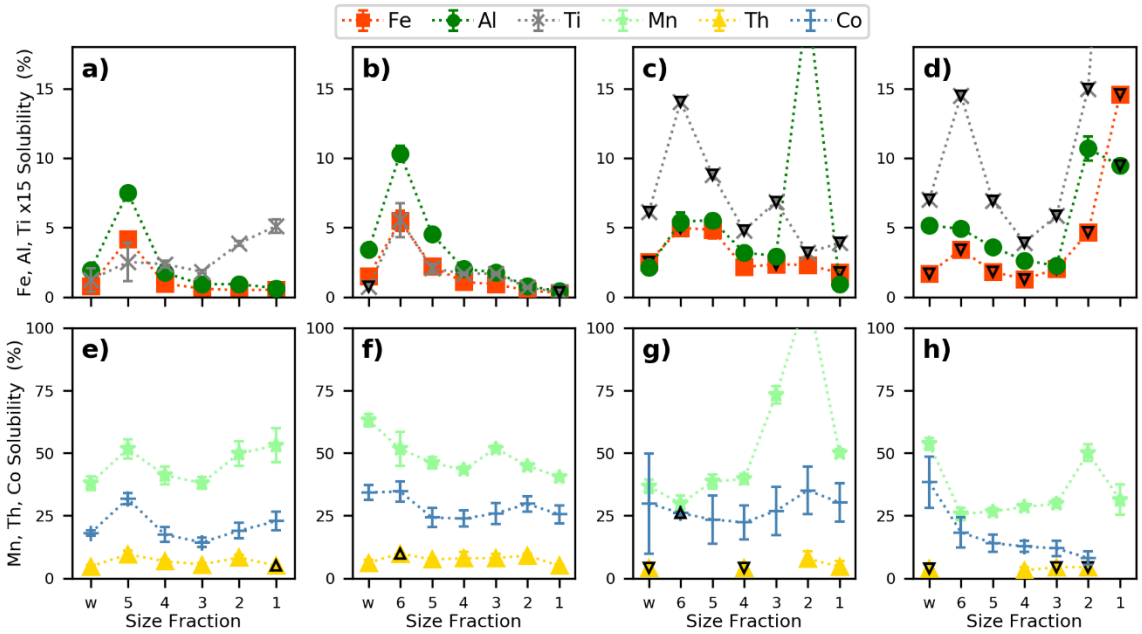

Figure 4 Fractional solubility (%) of elements in each aerosol size fraction for samples M15 (a & e), TM07 (b & f), TM25 (c & g) and TM26 (d & h). Ti solubility is increased 15-fold for clarity. Upward- and downward-pointing triangles on individual markers indicate that the plotted values are minima or maxima, respectively.

3.4 Influences on dust solubility

The enhancement of solubility in fine dust fractions for Fe, Al and Ti, and the absence of such enhancement for Mn, Co and Th, is intriguing, especially since these groups of elements are the same as those which do, and do not, exhibit hyperbolic changes in overall solubility with changing atmospheric dust (and total element) concentrations (Figure 2). A variety of proposed mechanisms could potentially account for the observed solubility – total atmospheric

concentration behaviour: mixing of dust with fine, high-solubility anthropogenic aerosol (as suggested for Fe (Sedwick et al., 2007; Sholkovitz et al., 2009)); acid-processing of dust particles during atmospheric transport (Spokes et al., 1994); preferential removal of larger, lower-solubility particles during atmospheric transport (Baker & Jickells, 2006).

The information available from the samples studied here is insufficient to determine unambiguously whether any one of these mechanisms dominates their solubility behaviour. If inclusion of anthropogenic Fe makes a significant contribution to the solubility of samples TM07 and M15, then similar high-solubility anthropogenic sources of Al (and Ti) would also be required to account for their observed solubility in these samples. This seems unlikely, but cannot be discounted without further evidence on anthropogenic emissions of the latter elements. Changes in mineral particle size distribution with transport cannot account for the particle size-dependent variation of solubility within each sample.

Acid processing provides a plausible mechanism which could be responsible for the similar enhancement of Fe, Al and Ti solubility in the fine fractions of samples TM07 and M15. Figure 5 shows the distributions of the major acid species (nitrate, non-seasalt sulphate and oxalate) in all of the aerosol samples. Nitrate was present predominantly on the larger size fractions, most probably as a result of the uptake of HNO_3 into seasalt particles and the subsequent displacement of HCl (Andreae & Crutzen, 1997). Thus acidity arising from nitrate probably does not play a role in the enhancement of Fe and Al solubility in the finer fractions of the dusty samples. The size distributions of nss-SO_4^{2-} show higher concentrations in the finer fractions, although there were noticeably higher proportions in the larger size fractions in the dusty samples (Figure 5a & b). The > 1 μm size fractions accounted for 42%, 56%, 10% and 20% of total nss-SO_4^{2-} in samples M15, TM07, TM25 and TM26 respectively. These distributions might be a result of the higher particle surface area available for SO_2 uptake when dust is present in high concentrations. Fang et al. (2017) reported enhanced solubility of Cu and Fe in aerosol size fractions where the populations of (fine mode) SO_4^{2-} and coarser particle total Cu and Fe overlap in urban aerosols. This change in solubility appeared to be linked to a large change in pH between the < 2.5 μm aerosol (pH < 2) and the coarser fractions (pH > 6), and resulted in the soluble metals being distributed on smaller particles than their total metals (Fang et al., 2017), as is observed for Fe, Al and Ti in the dusty samples here. Similar dependence on pH changes driven by the distribution of nss-SO_4^{2-} may be responsible for the enhanced solubility of Fe, Al and Ti

observed in samples M15 and TM07. Interestingly, Fang et al. (2017) also reported that there was much less difference between the size distributions of soluble and total Mn than for Cu and Fe, suggesting that Mn solubility has a weaker dependence on pH or that its solubilisation occurs via a different mechanism. Although complexation with oxalate can stabilise dissolved Fe (Paris et al., 2011), the distribution of oxalate does not appear to be related to the enhanced concentrations of soluble Fe in the dusty samples.

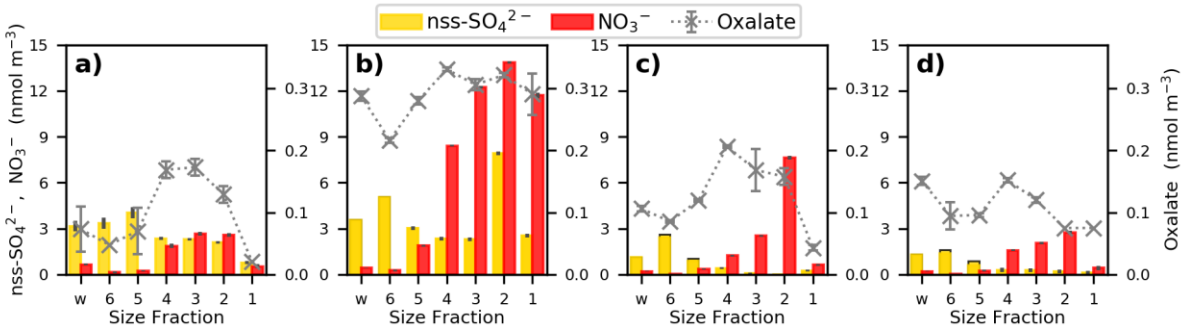

Figure 5 Concentrations of non-seasalt sulphate, nitrate and oxalate in each aerosol size fraction for samples M15 (a), TM07 (b), TM25 (c) and TM26 (d). Black caps on nss-SO_4^{2-} concentration bars (e.g. stages 5 & 6 in d)) indicate the uncertainty due to Na^+ concentrations being undetectable.

Whatever the cause of the higher solubility of Fe, Al and Ti in the fine fractions of the dusty samples, it is apparent that it does not result in similar enhancement in the solubility of Mn, Co and Th (Figure 4e & f). Weathering in arid environments produces mineral phases that have quite distinct geochemical compositions that are enriched in Mn, such as desert varnishes (Potter & Rossman, 1979) and these phases have been found coating Saharan dust particles collected at Barbados (Rydell & Prospero, 1972). Manganese oxides in soils are also noted to be associated with Co (Krauskopf & Bird, 1995). If Mn-enriched weathering products are present in Saharan dust aerosols, their size distribution appears to be similar to those of the principal Fe-, Al- and Ti- bearing minerals (Figure 3a & b). Whether such Mn-enriched minerals are associated with Co and Th, and how their dissolution behaviour differs from that of Fe-bearing minerals, is a subject for further study. Although Th solubility in a small number of other Saharan dust aerosol samples has been reported (Anderson et al., 2016), there does not appear to be any data, other than that reported here, with which to assess the variation of Th solubility with dust concentration changes during atmospheric transport. However, the similarity in the behaviour of

Mn and Th reported here suggests that the fractional solubility of Th over large gradients in dust concentration might be relatively constant. This would simplify the use of seawater Th concentration as a proxy for dust deposition flux (Hsieh et al., 2011), by reducing uncertainties in this term with respect to proxies (such as Al) that have hyperbolic solubility – concentration relationships.

4 Conclusions

Separation of two Saharan dust aerosol samples collected over the tropical Atlantic Ocean into multiple size fractions has demonstrated that the two groups of dust-associated trace metals (Fe, Al, Ti and Mn, Co, Th) show very different solubility characteristics in the particle size range 0.61 – 3.3 µm. The former group have enhanced solubility in this size range, while the latter do not. The solubility of these two groups also differs over large gradients in their total atmospheric concentration (as Saharan dust is transported over long distances in the atmosphere). The presence of Mn-enriched mineral phases in desert soils, and the association of Co with Mn minerals, might go some way to explaining the differences in solubility between these two groups of elements, and the unusual behaviour of Mn, Co and Th solubility in Saharan dust aerosols during atmospheric transport (Jickells et al., 2016; Shelley et al., 2018), but further work is necessary to confirm this.

Acknowledgments and Data

This work was supported by the UK Natural Environment Research Council, through grant numbers NE/H00548X/1 (UK GEOTRACES) and NE/F017359/1, and the University of East Anglia. We thank Eric Achterberg and Glen Tarran, chief scientists of the D361 and AMT21 cruises, Chan Yodle for collection of the AMT21 samples and analysis of major ions in sample M15 and the Masters and crews of RRS *Discovery*. We gratefully acknowledge the NOAA Air Resources Laboratory (ARL) for the provision of the HYSPLIT transport and dispersion model and READY website (http://www.arl.noaa.gov/ready.html) used in this publication. The authors declare that they have no conflict of interest. The data used in this publication is available from the British Oceanographic Data Centre (https://www.bodc.ac.uk/projects/data_management/uk/amt/data_delivery/ (AMT21) and https://www.bodc.ac.uk/geotraces/ (D361)) and the SOLAS Aerosol and Rain Composition database (https://www.bodc.ac.uk/solas_integration/implementation_products/group1/aerosol_rain/).

References

Aguilar-Islas, A. M., Wu, J. F., Rember, R., Johansen, A. M., & Shank, L. M. (2010). Dissolution of aerosol-derived iron in seawater: leach solution chemistry, aerosol type, and colloidal iron fraction. *Marine Chemistry, 120*(1-4), 25-33.

Anderson, R. F., Cheng, H., Edwards, R. L., Fleisher, M. Q., Hayes, C. T., Huang, K.-F., et al. (2016). How well can we quantify dust deposition to the ocean? *Philosophical Transactions A, 374*(2081), 20150285.

Andreae, M. O., & Crutzen, P. J. (1997). Atmospheric aerosols: Biogeochemical sources and role in atmospheric chemistry. *Science, 276*, 1052-1058.

Baker, A. R., & Jickells, T. D. (2006). Mineral particle size as a control on aerosol iron solubility. *Geophysical Research Letters, 33*, L17608.

Baker, A. R., & Jickells, T. D. (2017). Atmospheric deposition of soluble trace elements along the Atlantic Meridional Transect (AMT). *Progress in Oceanography, 158*, 41-51.

Baker, A. R., Jickells, T. D., Witt, M., & Linge, K. L. (2006). Trends in the solubility of iron, aluminium, manganese and phosphorus in aerosol collected over the Atlantic Ocean. *Marine Chemistry, 98*(1), 43-58.

Baker, A. R., Laskina, O., & Grassian, V. H. (2014). Processing and ageing in the atmosphere. In P. Knippertz & J. B. Stuut (Eds.), *Mineral Dust: A key player in the Earth System* (pp. 75-92). Dordrecht: Springer.

Bridgestock, L., Rehkämper, M., Van de Flierdt, T., Murphy, K., Khondoker, R., Baker, A. R., et al. (2017). The Cd isotope composition of atmospheric aerosols from the tropical Atlantic Ocean. *Geophysical Research Letters, 44*.

Bridgestock, L., van de Flierdt, T., Rehkämper, M., Paul, M., Middag, R., Milne, A., et al. (2016). Return of naturally sourced Pb to Atlantic surface waters. *Nature Communications, 7*, 12921.

Buck, C. S., Landing, W. M., & Resing, J. A. (2010). Particle size and aerosol iron solubility: A high-resolution analysis of Atlantic aerosols. *Marine Chemistry, 120*(1-4), 14-24.

Chen, Y., & Siefert, R. L. (2004). Seasonal and spatial distributions and dry deposition fluxes of atmospheric total and labile iron over the tropical and subtropical North Atlantic Ocean. *Journal Of Geophysical Research-Atmospheres, 109*(D9), D09305.

Draxler, R. R., & Rolph, G. D. (2003). *HYSPLIT (HYbrid Single-Particle Lagrangian Integrated Trajectory) Model access via NOAA ARL READY Website (http://www.arl.noaa.gov/ready/hysplit4.html).* Retrieved from Silver Spring, MD:

Fang, T., Guo, H., Zeng, L., Verma, V., Nenes, A., & Weber, R. J. (2017). Highly acidic ambient particles, soluble metals, and oxidative potential: A link between sulfate and aerosol toxicity. *Environmental Science & Technology, 51*(5), 2611-2620.

Hsieh, Y. T., Henderson, G. M., & Thomas, A. L. (2011). Combining seawater ^{232}Th and ^{230}Th concentrations to determine dust fluxes to the surface ocean. *Earth and Planetary Science Letters, 312*(3-4), 280-290.

Jickells, T. D., An, Z. S., Anderson, K. K., Baker, A. R., Bergametti, G., Brooks, N., et al. (2005). Global Iron Connections between desert dust, ocean biogeochemistry and climate. *Science, 308*, 67-71.

Jickells, T. D., Baker, A. R., & Chance, R. (2016). Atmospheric transport of trace elements and nutrients to the oceans. *Philosophical Transactions of the Royal Society of London Series A-Mathematical Physical and Engineering Sciences, 374*, 20150286.

Krauskopf, K. B., & Bird, D. K. (1995). *Introduction to geochemistry*. New York: McGraw-Hill Inc.

Mahowald, N. M., Hamilton, D. S., Mackey, K. R. M., Moore, J. K., Baker, A. R., Scanza, R. A., & Zhang, Y. (2018). Aerosol trace metal leaching and impacts on marine microorganisms. *Nature Communications, 9*, 2614.

385 Measures, C. I., Sato, T., Vink, S., Howell, S., & Li, Y. H. (2010). The fractional solubility of
386 aluminium from mineral aerosols collected in Hawaii and implications for atmospheric
387 deposition of biogeochemically important trace elements. *Marine Chemistry, 120*(1-4), 144-
388 153.
389 Morel, F. M. M., Kustka, A. B., & Shaked, Y. (2008). The role of unchelated Fe in the iron
390 nutrition of phytoplankton. *Limnology and Oceanography, 53*(1), 400-404.
391 Ooki, A., Nishioka, J., Ono, T., & Noriki, S. (2009). Size dependence of iron solubility of Asian
392 mineral dust particles. *Journal Of Geophysical Research, 114*, D03202.
393 Paris, R., Desboeufs, K. V., & Journet, E. (2011). Variability of dust iron solubility in
394 atmospheric waters: Investigation of the role of oxalate organic complexation. *Atmospheric*
395 *Environment, 45*(36), 6510-6517.
396 Potter, R. M., & Rossman, G. R. (1979). The manganese- and iron-oxide mineralogy of desert
397 varnish. *Chemical Geology, 25*(1-2), 79-94.
398 Prospero, J. M., Nees, R. T., & Uematsu, M. (1987). Deposition rate of particulate and dissolved
399 aluminum derived from Saharan dust in precipitation at Miami, Florida. *Journal Of*
400 *Geophysical Research, 92*(D12), 14,723–714,731.
401 Rydell, H. S., & Prospero, J. M. (1972). Uranium and thorium concentrations in wind-borne
402 Saharan dust over western equatorial North Atlantic Ocean. *Earth and Planetary Science*
403 *Letters, 14*(3), 397-402.
404 Ryder, C. L., Highwood, E. J., Lai, T. M., Sodemann, H., & Marsham, J. H. (2013). Impact of
405 atmospheric transport on the evolution of microphysical and optical properties of Saharan
406 dust. *Geophysical Research Letters, 40*(10), 2433-2438.
407 Sakata, K., Kurisu, M., Tanimoto, H., Sakaguchi, A., Uematsu, M., Miyamoto, C., & Takahashi,
408 Y. (2018). Custom-made PTFE filters for ultra-clean size-fractionated aerosol sampling for
409 trace metals. *Marine Chemistry, 206*, 100-108.
410 Sedwick, P. N., Sholkovitz, E. R., & Church, T. M. (2007). Impact of anthropogenic combustion
411 emissions on the fractional solubility of aerosol iron: Evidence from the Sargasso Sea.
412 *Geochemistry Geophysics Geosystems, 8*, Q10Q06.
413 Shelley, R. U., Landing, W. M., Ussher, S. J., Planquette, H., & Sarthou, G. (2018). Regional
414 trends in the fractional solubility of Fe and other metals from North Atlantic aerosols
415 (GEOTRACES cruises GA01 and GA03) following a two-stage leach. *Biogeosciences, 15*(7),
416 2271-2288.
417 Sholkovitz, E. R., Sedwick, P. N., & Church, T. M. (2009). Influence of anthropogenic
418 combustion emissions on the deposition of soluble aerosol iron to the ocean: Empirical
419 estimates for island sites in the North Atlantic. *Geochimica Et Cosmochimica Acta, 73*, 3981-
420 4003.
421 Sholkovitz, E. R., Sedwick, P. N., Church, T. M., Baker, A. R., & Powell, C. F. (2012).
422 Fractional solubility of aerosol iron: Synthesis of a global-scale data set. *Geochimica Et*
423 *Cosmochimica Acta, 89*, 173-189.
424 Spokes, L. J., Jickells, T. D., & Lim, B. (1994). Solubilisation of aerosol trace metals by cloud
425 processing: A laboratory study. *Geochimica Et Cosmochimica Acta, 58*, 3281-3287.
426 Stuut, J. B., Zabel, M., Ratmeyer, V., Helmke, P., Schefuss, E., Lavik, G., & Schneider, R.
427 (2005). Provenance of present-day eolian dust collected off NW Africa. *Journal Of*
428 *Geophysical Research-Atmospheres, 110*(D4), D04202.

429